

Near-Field Localization with Dynamic Metasurface Antennas at THz: A CRB Minimizing Approach

Ioannis Gavras, *Student Member, IEEE*, and George C. Alexandropoulos, *Senior Member, IEEE*

Abstract—The recent trend for extremely massive antenna arrays and high frequencies facilitates localization and sensing, offering increased angular and range resolution. In this letter, we focus on the emerging technology of Dynamic Metasurface Antennas (DMAs) and present a novel framework for the design of their analog beamforming weights, targeting high accuracy near-field localization at the THz frequency band. We derive the Cramér-Rao Bound (CRB) for the estimation of the positions of multiple users with a DMA-based receiver, which is then utilized as the optimization objective for the receiver's discrete tunable states of its metamaterials. Leveraging the DMA structure, we reformulate the localization objective into a constrained Rayleigh quotient maximization problem, which is efficiently solved via two schemes: one based on projection and a greedy one. Our simulation results verify the validity of our near-field localization analysis, showcasing the effectiveness of the proposed near-field localization designs over the optimum exhaustive search solution and state-of-the-art schemes.

Index Terms—Dynamic metasurfaces antennas, beamforming, Cramér-Rao bound, localization, near-field, THz.

I. INTRODUCTION

Extremely large antenna arrays are expected to be widely deployed in next generation wireless networks [1]–[3], especially for high-frequency systems [4], offering numerous spatial degrees of freedom for communications, localization, and sensing applications. Dynamic Metasurface Antennas (DMAs) constitute a recent power- and cost-efficient hybrid analog and digital transceiver architecture utilizing arbitrary large numbers of phase-tunable metamaterials, which are grouped in disjoint microstrips each attached to a Radio Frequency (RF) chain and are capable for realizing analog transmit or Receive (RX) BeamForming (BF) [5].

The beam focusing capability of a DMA-based transmitter serving multiple User Equipment (UE) lying within its near-field regime was optimized in [6]. An autoregressive attention neural network for non-line-of-sight user tracking with an RX DMA was devised in [7], while [8] presented a near-field beam tracking framework for the same RX architecture. An approach for configuring the analog DMA weights for near-field localization was proposed in [9], by reformulating the original localization objective as a received signal strength improvement one. Very recently, in [10], [11], focusing on

near-field scenarios in the THz frequency band, designs for the digital and analog BF matrices of DMA-based full duplex transceivers were presented targeting integrated sensing and communications. However, unlike other BF architectures, such as networks of phase shifters and movable antennas [12]–[14], and to the best of our knowledge, the explicit optimization of DMAs for near-field localization has not yet been studied.

In this letter, we study the optimization of DMA-based reception for multi-UE near-field localization, focusing on THz frequencies. We first derive the Cramér-Rao Bound (CRB) for the estimation of the UEs' range and angular parameters as well as the position error bound (PEB), and then utilize the minimization of the former as the objective for the design of the DMA analog RX BF weights. Leveraging the partially-connected analog BF architecture of the RX DMA, we reformulate its design objective into a Rayleigh quotient optimization problem with discrete constraints onto the analog BF weights, which is efficiently solved. Our simulation results on a sub-THz narrowband channel verify the validity of our near-field localization analysis, showcasing the superiority of our presented localization-optimized DMA design over conventional ones, when all combined with Maximum Likelihood Estimation (MLE).

Notations: Vectors and matrices are represented by boldface lowercase and uppercase letters, respectively. The transpose, Hermitian transpose, inverse, and Euclidean norm are denoted as $(\cdot)^T$, $(\cdot)^H$, $(\cdot)^{-1}$, and $\|\cdot\|$, respectively. $[\mathbf{A}]_{i,j}$ and $[\mathbf{A}]_{i:j,u:v}$ give respectively \mathbf{A} 's (i,j) th element and sub-matrix spanning rows i to j and columns u to v . \mathbf{I}_n and $\mathbf{0}_n$ ($n \geq 2$) are the $n \times n$ identity and zeros' matrices, respectively, and $\mathbf{1}_N$ is an $N \times 1$ column vector of ones. \mathbb{C} is the complex number set, $|a|$ is the amplitude of scalar a , and $j \triangleq \sqrt{-1}$. $\mathbb{E}\{\cdot\}$, $\text{Tr}\{\cdot\}$, and $\text{Re}\{\cdot\}$ give the expectation, trace, and real part, respectively. ∇ is the vector differential operator, \circ is the Hadamard product, and $\mathbf{x} \sim \mathcal{CN}(\mathbf{a}, \mathbf{A})$ indicates a complex Gaussian random vector with mean \mathbf{a} and covariance matrix \mathbf{A} .

II. SYSTEM AND CHANNEL MODELS

We consider an RX equipped with a DMA panel [5] wishing to localize U single-antenna UEs placed within its effective coverage area. DMAs efficiently enable the integration of numerous sub-wavelength-spaced metamaterials, which are usually grouped in microstrips each attached to a reception RF chain (comprising a low noise amplifier, a mixer downconverting the received signal from RF to baseband, and an analog-to-digital converter), within possibly extremely large apertures [2]. By dynamically tuning the responses of metamaterials in the impinging/received signal, goal-oriented analog RX BF (in this paper, localization) can be realized.

This work has been supported by the SNS JU project TERRAMETA under the EU's Horizon Europe research and innovation programme under Grant Agreement No 101097101, including top-up UKRI funding under the UK government's Horizon Europe funding guarantee.

The authors are with the Department of Informatics and Telecommunications, National and Kapodistrian University of Athens, 16122 Athens, Greece. G. C. Alexandropoulos is also with the Department of Electrical and Computer Engineering, University of Illinois Chicago, IL 60601, USA (e-mails: {giannisgav, alexandg}@di.uoa.gr).

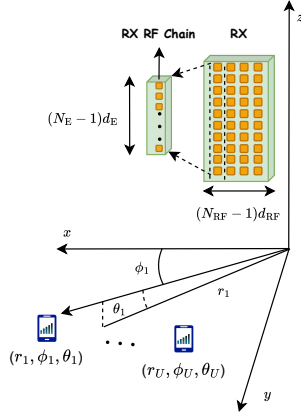


Fig. 1: The considered DMA-equipped RX, including its geometry and the adopted coordinate system, used for near-field localization.

As depicted in Fig. 1, the RX DMA panel is situated in the xz -plane with the first microstrip positioned at the origin. There exist in total N_{RF} microstrips within the panel, each composed of N_E distinct metamaterials placed in a uniform linear pattern with d_E distance between adjacent elements. The microstrips are individually linked to reception RF chains, which are separated from one another by a distance of d_{RF} . Consequently, the RX DMA includes in total $N \triangleq N_{\text{RF}}N_E$ metamaterials. The position of each u th ($u = 1, \dots, U$) UE is expressed in spherical coordinates as (r_u, θ_u, ϕ_u) , including respectively its distance from the origin of the coordinate system in Fig. 1 as well as the elevation and azimuth angles.

We define the $N \times N$ diagonal matrix \mathbf{P}_{RX} , with elements modeling signal propagation inside the RX DMA's microstrips, as follows $\forall i = 1, \dots, N_{\text{RF}}$ and $\forall n = 1, \dots, N_E$ [10]:

$$[\mathbf{P}_{\text{RX}}]_{(i-1)N_E+n, (i-1)N_E+n} \triangleq \exp(-\rho_{i,n}(\alpha_i + j\beta_i)), \quad (1)$$

where α_i represents the waveguide attenuation coefficient, β_i stands for the wavenumber, and $\rho_{i,n}$ signifies the position of the n th element within the i th microstrip. Let also $w_{i,n}^{\text{RX}}$ be the adjustable response (i.e., analog weight), associated with each n th metamaterial in each i th microstrip. This weight is assumed to conform to a Lorentzian-constrained phase model and is assumed to belong to the phase profile codebook \mathcal{W} :

$$w_{i,n}^{\text{RX}} \in \mathcal{W} \triangleq \{0.5(j + e^{j\phi}) \mid \phi \in [-\pi/2, \pi/2]\}. \quad (2)$$

Using this definition, the DMA's analog RX BF matrix $\mathbf{W}_{\text{RX}} \in \mathbb{C}^{N \times N_{\text{RF}}}$ is obtained as $[\mathbf{W}_{\text{RX}}]_{(i-1)N_E+n, j} = w_{i,n}^{\text{RX}}$ for $i = j$, and as $[\mathbf{W}_{\text{RX}}]_{(i-1)N_E+n, j} = 0$ for $i \neq j$.

A. Near-Field Channel Model

We study wireless operations in the THz frequency band and within a near-field signal propagation environment [4]. The N -element complex-valued vector channel between the RX DMA and each u th single-antenna UE is modeled as follows:

$$[\mathbf{h}_u]_{(i-1)N_E+n} \triangleq \alpha_{u,i,n} \exp\left(\frac{j2\pi}{\lambda} r_{u,i,n}\right), \quad (3)$$

where $r_{u,i,n}$ denotes the distance from the u th UE to the n th metamaterial of the i th microstrip (and respective RF

chain) of the RX DMA panel. The attenuation factor $\alpha_{u,i,n}$ accommodates molecular absorption with a coefficient of κ_{abs} in the THz range, and is formally expressed via the formula:

$$\alpha_{u,i,n} \triangleq \sqrt{F(\theta_{u,i,n})} \frac{\lambda}{4\pi r_{u,i,n}} \exp\left(-\frac{\kappa_{\text{abs}} r_{u,i,n}}{2}\right) \quad (4)$$

with λ being the wavelength and $F(\cdot)$ is each metamaterial's radiation profile, modeled for an elevation angle θ as follows:

$$F(\theta) = \begin{cases} 2(b+1)\cos^b(\theta), & \text{if } \theta \in [-\frac{\pi}{2}, \frac{\pi}{2}], \\ 0, & \text{otherwise.} \end{cases} \quad (5)$$

In the latter expression, b determines the boresight antenna gain which depends on the specific DMA technology [5]. It is finally noted that each distance $r_{u,i,n}$ in (3) and (4) can be calculated, using the coordinate system in Fig. 1, as follows:

$$r_{u,i,n} = \left((r_u \sin \theta_u \cos \phi_u - (i-1)d_{\text{RF}})^2 + (r_u \sin \theta_u \sin \phi_u)^2 + (r_u \cos \theta_u - (n-1)d_E)^2 \right)^{\frac{1}{2}}. \quad (6)$$

The elevation angle of each u th UE's antenna with respect to each n th element of each i th microstrip is expressed as:

$$\theta_{u,i,n} \triangleq \sin^{-1} \left(r_{u,i,n}^{-1} |(n-1)d_E - r_u \cos \theta_u| \right). \quad (7)$$

B. Received Signal Model

The baseband received signals at the outputs of the RX DMA's RF chains after T UE pilot transmissions can be mathematically expressed via the matrix $\mathbf{Y} \triangleq [\mathbf{y}(1), \dots, \mathbf{y}(T)] \in \mathbb{C}^{N_{\text{RF}} \times T}$ with $t = 1, \dots, T$:

$$\mathbf{Y} = \mathbf{W}_{\text{RX}}^H \mathbf{P}_{\text{RX}}^H \sum_{u=1}^U \mathbf{h}_u^H \mathbf{s}_u + \mathbf{W}_{\text{RX}}^H \mathbf{P}_{\text{RX}}^H \mathbf{N}, \quad (8)$$

where $\mathbf{N} \triangleq [\mathbf{n}(1), \dots, \mathbf{n}(T)] \in \mathbb{C}^{N \times T}$ with each $\mathbf{n}(t) \sim \mathcal{CN}(\mathbf{0}, \sigma^2 \mathbf{I}_{N_{\text{RF}}})$ being the Additive White Gaussian Noise (AWGN) vector, and $\mathbf{s}_u \triangleq [s_u(1), \dots, s_u(T)] \in \mathbb{C}^{1 \times T}$. Each transmitted pilot signal $s_u(t)$ is subjected to the power constraint $\mathbb{E}\{\|s_u(t)\|^2\} \leq P_{\text{max}}$, where P_{max} signifies the common maximum UE transmission power in the uplink.

III. DMA DESIGN FOR NEAR-FIELD LOCALIZATION

In this section, we present our RX DMA design for near-field localization. We first derive the CRB and PEB for the intended estimation, which are used for our design objective formulation. Finally, our solution for the DMA's analog BF weights is presented along with its computational complexity.

A. PEB Analysis

It is evident from (8)'s inspection that, for a sufficiently large number T of pilot transmissions per UE within a coherent channel block, yields $T^{-1} \mathbb{E}\{\mathbf{s}_u \mathbf{s}_u^H\} = P_{\text{max}} \mathbf{I}_{N_{\text{RF}}} \forall u$, indicating that the received signal at the DMA's RF chains is distributed as $\mathbf{Y} \sim \mathcal{CN}(\mathbf{M}, \mathbf{R}_n)$ with mean $\mathbf{M} \triangleq \mathbf{W}_{\text{RX}}^H \mathbf{P}_{\text{RX}}^H \sum_{u=1}^U \mathbf{h}_u^H \mathbf{s}_u$ and covariance $\mathbf{R}_n \triangleq \sigma^2 \mathbf{W}_{\text{RX}}^H \mathbf{P}_{\text{RX}}^H \mathbf{P}_{\text{RX}} \mathbf{W}_{\text{RX}} \mathbf{I}_{N_{\text{RF}}}$. By defining the vector $\boldsymbol{\zeta} \triangleq [r_1, \theta_1, \phi_1, \dots, r_U, \theta_U, \phi_U]^T$ with the parameters of the true

UE positions, the $3UT \times 3UT$ Fisher Information Matrix (FIM) for its estimation can be calculated as follows [11]:

$$\mathcal{I} = \begin{bmatrix} \mathcal{I}_{r_1 r_1} & \mathcal{I}_{r_1 \theta_1} & \mathcal{I}_{r_1 \phi_1} & \dots & \mathcal{I}_{r_1 \phi_U} \\ \mathcal{I}_{\theta_1 r_1} & \mathcal{I}_{\theta_1 \theta_1} & \mathcal{I}_{\theta_1 \phi_1} & \dots & \mathcal{I}_{\theta_1 \phi_U} \\ \mathcal{I}_{\phi_1 r_1} & \mathcal{I}_{\phi_1 \theta_1} & \mathcal{I}_{\phi_1 \phi_1} & \dots & \mathcal{I}_{\phi_1 \phi_U} \\ \vdots & \vdots & \vdots & \ddots & \vdots \\ \mathcal{I}_{\phi_U r_1} & \mathcal{I}_{\phi_U \theta_1} & \mathcal{I}_{\phi_U \phi_1} & \dots & \mathcal{I}_{\phi_U \phi_U} \end{bmatrix}, \quad (9)$$

where each (i, j) th $(i, j = 1, \dots, 3U)$ matrix element $[\mathcal{I}]_{i,j}$ of size $T \times T$ is given by:

$$[\mathcal{I}]_{i,j} = 2\text{Re} \left\{ \frac{\partial \mathbf{M}^H}{\partial [\zeta]_i} \mathbf{R}_n^{-1} \frac{\partial \mathbf{M}}{\partial [\zeta]_j} \right\} + \text{Tr} \left\{ \mathbf{R}_n^{-1} \frac{\partial \mathbf{R}_n}{\partial [\zeta]_i} \mathbf{R}_n^{-1} \frac{\partial \mathbf{R}_n}{\partial [\zeta]_j} \right\}.$$

Since $\nabla_{\zeta} \mathbf{R}_n = \mathbf{0}_{3U \times 1}$ due to the fact that \mathbf{R}_n is independent of ζ , it holds that each FIM value depends solely on \mathbf{Y} 's mean value. We next compute the following derivative $\forall i$:

$$\frac{\partial \mathbf{M}}{\partial [\zeta]_i} = \mathbf{W}_{\text{RX}}^H \mathbf{P}_{\text{RX}}^H \sum_{u=1}^U \frac{\partial \mathbf{h}_u^H}{\partial [\zeta]_i} \mathbf{s}_u. \quad (10)$$

Consequently, each diagonal element of the FIM matrix in (9) can be expressed as follows with $\mathbf{F} \triangleq \mathbf{W}_{\text{RX}} \mathbf{R}_n^{-1} \mathbf{W}_{\text{RX}}^H$:

$$[\mathcal{I}]_{i,i} = 2 \sum_{u=1}^U \text{Re} \left\{ \mathbf{s}_u^H \frac{\partial \mathbf{h}_u}{\partial [\zeta]_i} \mathbf{P}_{\text{RX}} \mathbf{F} \mathbf{P}_{\text{RX}}^H \frac{\partial \mathbf{h}_u^H}{\partial [\zeta]_i} \mathbf{s}_u \right\}. \quad (11)$$

Putting all above together, the sum-PEB with respect to all UEs' with polar coordinates $\{(r_1, \theta_1, \phi_1), \dots, (r_U, \theta_U, \phi_U)\}$, considering an RX DMA, is given by [15]:

$$\text{PEB}_{\zeta} \triangleq \sqrt{\text{CRB}_{\zeta}} = \sqrt{\text{Tr} \{ \mathcal{I}^{-1} \}}. \quad (12)$$

B. DMA Design Objective

Our goal, in this paper, is to optimize the RX DMA's analog BF weights for facilitating the localization of multiple UEs lying in its near-field region. To this end, we leverage the positive semidefinite nature of the FIM and the lower bound $\text{Tr} \{ \mathcal{I}^{-1} \} \geq \frac{9U^2 T^2}{\text{Tr} \{ \mathcal{I} \}}$ resulting from the following proposition.

Proposition 1 (Inequality for positive semidefinite matrices). *For any $N \times N$ complex positive semidefinite and invertible matrix \mathcal{K} , the inequality $\text{Tr} \{ \mathcal{K}^{-1} \} \geq \frac{N^2}{\text{Tr} \{ \mathcal{K} \}}$ holds.*

Proof. Let $\lambda_1, \dots, \lambda_N \geq 0$ be \mathcal{K} 's eigenvalues, yielding the expressions $\text{Tr} \{ \mathcal{K} \} = \sum_{i=1}^N \lambda_i$ and $\text{Tr} \{ \mathcal{K}^{-1} \} = \sum_{i=1}^N \lambda_i^{-1}$. It is deduced from the harmonic-geometric mean inequality:

$$\frac{N}{\sum_{i=1}^N \lambda_i^{-1}} \leq \frac{\sum_{i=1}^N \lambda_i}{N} \Leftrightarrow \sum_{i=1}^N \lambda_i^{-1} \geq \frac{N^2}{\sum_{i=1}^N \lambda_i}.$$

Substituting the previous trace definitions for \mathcal{K} and its inverse in the latter inequality, completes the proof. \square

We now focus on the minimization of the latter lower bound for the estimation of the UEs' positions parameter vector ζ , which can be mathematically formulated via the optimization:

$$\mathcal{OP} : \max_{\mathbf{W}_{\text{RX}}} \text{Tr} \{ \mathcal{I} \} \quad \text{s.t. } w_{i,n}^{\text{RX}} \in \mathcal{W} \quad \forall i, n.$$

We next use the vector definitions $\mathbf{a}_u \triangleq \mathbf{P}_{\text{RX}}^H \frac{\partial \mathbf{h}_u^H}{\partial r_u}$, $\mathbf{b}_u \triangleq \mathbf{P}_{\text{RX}}^H \frac{\partial \mathbf{h}_u^H}{\partial \theta_u}$, and $\mathbf{c}_u \triangleq \mathbf{P}_{\text{RX}}^H \frac{\partial \mathbf{h}_u^H}{\partial \phi_u}$, to simplify \mathcal{OP} 's objective as follows: $\text{Tr} \left\{ \text{Re} \left\{ \left(\sum_{u=1}^U \mathbf{a}_u \mathbf{a}_u^H + \mathbf{b}_u \mathbf{b}_u^H + \mathbf{c}_u \mathbf{c}_u^H \right) \mathbf{F} \right\} \right\}$.

Algorithm 1 Projection-Based Solution for \mathcal{OP}

Input: Initialization for \mathbf{W}_{RX} , \mathbf{P}_{RX} , \mathcal{W} , and initial estimate for ζ .

Output: \mathbf{W}_{RX} .

- 1: Construct \mathbf{Q} and solve $\mathcal{OP}_i \quad \forall i$ to obtain \mathbf{q}_i 's. Then, compute each i th Lorentzian-constrained vector via the expression $\bar{\mathbf{w}}_i = 0.5(j\mathbf{1}_{N_E} + \mathbf{q}_i)$.
- 2: Project each $\bar{\mathbf{w}}_i$ onto the codebook \mathcal{W} via an one-dimensional search using (16).

C. Proposed Analog RX BF for Near-Field Localization

Profiting from the partially-connected analog RX BF architecture of the DMA [5], \mathbf{Y} 's covariance matrix \mathbf{R}_n is a diagonal matrix with the following distinctive composition:

$$\mathbf{R}_n = \sigma^2 \text{diag} \{ (\mathbf{w}_1^H \circ \mathbf{p}_1^H) (\mathbf{p}_1 \circ \mathbf{w}_1), \dots, (\mathbf{w}_{N_{\text{RF}}}^H \circ \mathbf{p}_{N_{\text{RF}}}^H) (\mathbf{p}_{N_{\text{RF}}} \circ \mathbf{w}_{N_{\text{RF}}}) \}, \quad (13)$$

where $\forall i = 1, \dots, N_{\text{RF}}$ using $\kappa_i \triangleq (i-1)N_E + 1$:

$$\mathbf{p}_i \triangleq [\text{diag}(\mathbf{P}_{\text{RX}})]_{\kappa_i:iN_E}, \quad \mathbf{w}_i \triangleq [\mathbf{W}_{\text{RX}}]_{\kappa_i:iN_E, i}. \quad (14)$$

Consequently, it can be easily verified that matrix \mathbf{F} appearing in \mathcal{OP} 's simplified objective has a block diagonal structure with each block i (out of the N_{RF}) having the following form:

$$[\mathbf{F}]_{\kappa_i:iN_E, \kappa_i:iN_E} = \frac{\mathbf{w}_i \mathbf{w}_i^H}{\sigma^2 \|\mathbf{w}_i\|^2 \|\mathbf{p}_i\|^2}. \quad (15)$$

It can be easily shown for the matrix $\mathbf{Q} \triangleq \sum_{u=1}^U \mathbf{a}_u \mathbf{a}_u^H + \mathbf{b}_u \mathbf{b}_u^H + \mathbf{c}_u \mathbf{c}_u^H$ appearing in \mathcal{OP} 's simplified objective that it is a positive semidefinite matrix. Using this property and \mathbf{F} 's block diagonal structure, as shown in (15), \mathcal{OP} can be decomposed into the following N_{RF} sub-problems that can be solved in parallel:

$$\begin{aligned} \mathcal{OP}_i : \max_{\mathbf{w}_i} \text{Tr} \left\{ \text{Re} \left\{ \frac{\mathbf{w}_i^H [\mathbf{Q}]_{\kappa_i:iN_E, \kappa_i:iN_E} \mathbf{w}_i}{\|\mathbf{w}_i\|^2} \right\} \right\} \\ \text{s.t. } w_{i,n}^{\text{RX}} \in \mathcal{W} \quad \forall i, n. \end{aligned}$$

Clearly, each \mathcal{OP}_i deals with the maximization of a Rayleigh quotient [16], thus, the optimal solution for each \mathbf{w}_i , when neglecting the codebook-based constraint, is obtained from $[\mathbf{Q}]_{\kappa_i:iN_E, \kappa_i:iN_E}$'s principal singular vector, denoted by \mathbf{q}_i . Specifically, for each i th RF chain at the RX DMA, we can construct the optimal Lorentzian-constrained analog BF vector as $\bar{\mathbf{w}}_i \triangleq 0.5(j\mathbf{1}_{N_E} + \mathbf{q}_i)$. Then, to deal with each \mathcal{OP}_i 's constraint, we propose to project each $\bar{\mathbf{w}}_i$ onto the finite-sized codebook \mathcal{W} , and consequently seek via an one-dimensional search for the best N -element analog RX BF vector \mathbf{w} for the DMA, that is constructed from \mathcal{W} , minimizing the following vector distance criterion:

$$\mathbf{w}_i = \arg \min_{\mathbf{w}} \sqrt{1 - \left| \frac{\mathbf{w}^H \bar{\mathbf{w}}_i}{\|\mathbf{w}\| \|\bar{\mathbf{w}}_i\|} \right|}. \quad (16)$$

The complete algorithm for this projection-based solution of \mathcal{OP} is summarized in Algorithm 1.

Algorithm 2 Greedy-Based Solution for \mathcal{OP}

Input: Initialization for \mathbf{W}_{RX} , \mathbf{P}_{RX} , \mathcal{W} , and initial estimate for ζ .

Output: \mathbf{W}_{RX} .

- 1: Initialize the set \mathcal{S} with N_{RF} randomly selected codewords from \mathcal{W} , and set $\overline{\mathcal{W}} = \mathcal{W}$.
 - 2: **while** $\overline{\mathcal{W}}$ is not empty **do**
 - 3: Select a random codeword $\bar{\mathbf{w}}$ from $\overline{\mathcal{W}}$ and then remove it from this codebook.
 - 4: Determine whether $\bar{\mathbf{w}}$ can replace any codeword in the set \mathcal{S} to achieve a larger improvement \mathcal{OP} 's objective. If such a replacement is possible, update \mathcal{S} accordingly.
 - 5: **end while**
-

D. Computational Complexity Analysis

The optimal solution for \mathcal{OP} can be obtained by exhaustive search, which is computationally demanding with $\mathcal{O}(\binom{N_{\mathcal{W}}}{N_{\text{RF}}})$ of complexity, where $N_{\mathcal{W}}$ denotes the total number of analog RX BF vectors for the DMA that can be constructed from \mathcal{W} . On the other hand, our projection-based sub-optimal solution for all \mathcal{OP}_i 's presented in Section III-C needs smaller computational complexity of $\mathcal{O}(N_{\text{RF}}(N_{\text{E}}^3 + N_{\mathcal{W}}))$. Specifically, $\mathcal{O}(N_{\text{E}}^3)$ of complexity is required for the singular value decompositions of $[\mathbf{Q}]_{\kappa_i:iN_{\text{E}},\kappa_i:iN_{\text{E}}}$'s, while all projection steps need $\mathcal{O}(N_{\text{RF}}N_{\mathcal{W}})$ mathematical operations.

In the results that follow, we will also investigate the following greedy-based approach for solving \mathcal{OP} , which requires only $\mathcal{O}(N_{\mathcal{W}})$ of complexity. Starting with N_{RF} randomly selected analog RX BF vectors from \mathcal{W} , we continue with an additional random selection of a vector to replace any of the N_{RF} previous ones yielding the largest value for \mathcal{OP} 's objective function. Then, this selected vector is removed from \mathcal{W} . This process is repeated until all vectors from \mathcal{W} are selected. It is noted that, if $N_{\text{RF}} > N_{\mathcal{W}}$ holds, N_{RF} copies of codebook \mathcal{W} will be utilized for the greedy-based approach. The complete algorithm for the greedy-based solution of \mathcal{OP} is summarized in Algorithm 2.

IV. NUMERICAL RESULTS AND DISCUSSION

In this section, we numerically evaluate the performance of the proposed RX DMA design for near-field localization, when used in conjunction with the MLE scheme [17]. We have considered the scenario of Fig. 1 at 120 GHz central frequency with a $B = 150$ KHz bandwidth, including $U = 3$ single-antenna UEs lying in the DMA's near-field (Fresnel) region given by $\theta_u = 30^\circ$, $\phi_u \in [1^\circ, 90^\circ]$, and $r_u \in [1, 12]$ meters, $\forall u$. In the RX DMA, its microstrips and metamaterials were spaced with $d_{\text{RF}} = \frac{\lambda}{2}$ and $d_{\text{E}} = \frac{\lambda}{5}$, respectively. A 3-bit beam codebook \mathcal{W} was used, initially restricting all elements' phase responses to the set $\mathcal{F} \in \{e^{j\phi} | \phi \in [-\pi/2, \pi/2]\}$, having elements of constant unit amplitude and uniformly distributed phase values. Then, to compensate for the signal propagation inside the DMA microstrips, we set $w_{i,n}^{\text{RX}} = 0.5(j + \tilde{w}_{i,n}^{\text{RX}} e^{j\phi_{i,n}\beta_i})$ with $\tilde{w}_{i,n}^{\text{RX}} \in \mathcal{F} \forall i, n$. We have conducted 300 Monte Carlo simulations, each including $T = 100$ UE pilot transmissions, and set AWGN's variance as $\sigma^2 = -174 + 10\log_{10}(B)$ in dBm.

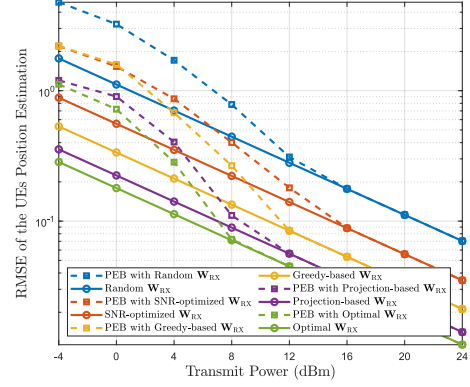


Fig. 2: Mean RMSE of the positions of the $U = 3$ UEs versus the transmit power P_{max} in dBm, considering an RX DMA with $N_{\text{RF}} = 4$ microstrips each consisting of $N_{\text{E}} = 256$ phase-tunable metamaterials.

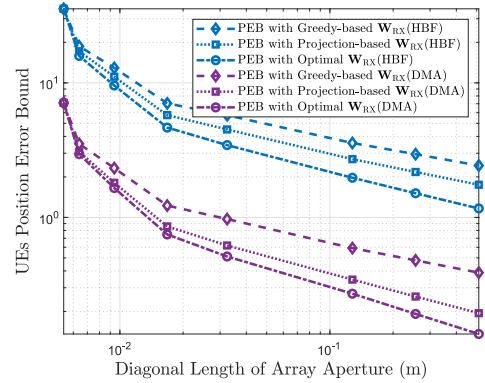


Fig. 3: PEB versus the diagonal length in meters of the RX antenna panel, considering a DMA and an HBF with $\lambda/5$ and $\lambda/2$ element spacing, respectively, each with $N_{\text{RF}} = 4$, and $P_{\text{max}} = -4$ dBm.

In Fig. 2, the Root Mean Square Error (RMSE) of the UE's position and the PEBs of the proposed projection- and greedy-based \mathbf{W}_{RX} designs are compared with that of the localization-based DMA design in [10] maximizing the received Signal-to-Noise Ratio (SNR), a scheme with a random \mathbf{W}_{RX} , and the optimal solution obtained through exhaustive search, when all considered to perform MLE at an RX DMA equipped with $N_{\text{RF}} = 4$ microstrips each hosting $N_{\text{E}} = 256$ phase-tunable elements. As expected, all RMSE curves improve with increasing P_{max} (i.e., SNR), converging to the respective PEBs. It is also shown that our optimization framework outperforms both that of [10] and randomized DMA reception, verifying the effectiveness of our near-field localization design. Notably, the proposed projection- and greedy-based approaches exhibit comparable performance with the optimal RX BF solution, making our greedy-based one more preferable for low complexity implementations.

Figure 3 illustrates the PEB performance of both proposed designs together with that of the optimal solution for \mathcal{OP} versus the diagonal length of the RX antenna panel for two antenna architectures each with $N_{\text{RF}} = 4$ reception RF chains: DMA and partially connected Hybrid analog and digital BF (HBF) with phase shifters (via Section III ignoring \mathbf{P}_{RX} and replacing \mathcal{W} with the columns of the discrete Fourier transform matrix). The inter-element spacing within each

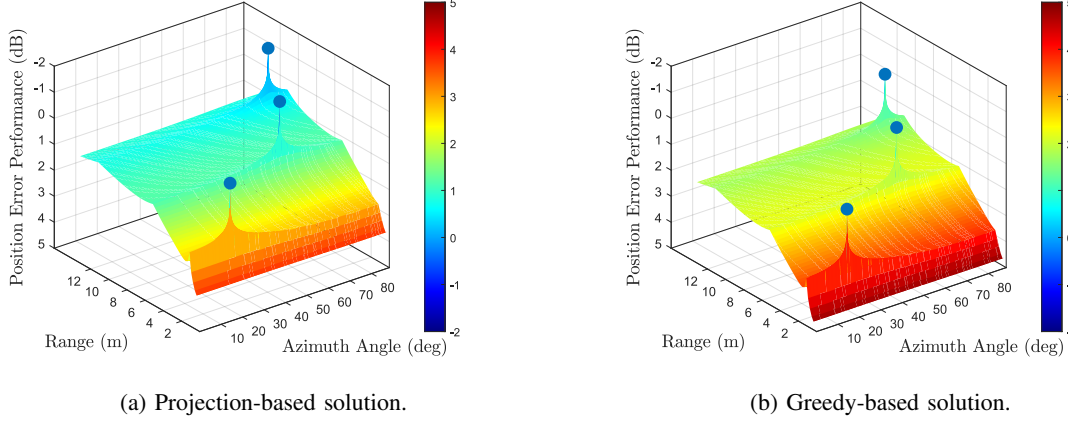


Fig. 4: Area-wide position estimation error with MLE for both proposed \mathbf{W}_{RX} designs (the vertical axes include error values in ascending order from the top to bottom), considering $U = 3$ UEs each using $P_{\text{max}} = 20$ dBm for pilot transmission, and the DMA configuration of Fig. 2. The blue markers in both subfigures indicate the true positions of the UEs.

microstrip of the former was chosen as $\lambda/5$, whereas, for the latter, $\lambda/2$ was the inter-element spacing of each single-RF-fed linear antenna array constituting the HBF. As expected, the denser element placement facilitated by the DMA architecture results in superior performance. It also shows that, as the size of the RX antenna panel increases, the gap between our projection-based design and the optimal solution (i.e., RX BF via exhaustive search) increases, with this gap being more pronounced for HBF for the same panel size.

The MLE error performance over a grid of pairs of range and azimuth angle values is illustrated in Fig. 4, considering the RX DMA of Fig. 2 and $P_{\text{max}} = 20$ dBm for each of the $U = 3$ UEs. Estimations of the true positions of the UEs with random analog RX BF initializations were used for both our optimized \mathbf{W}_{RX} design approaches, which were then combined with MLE for the entire grid. It can be observed in the figure that the estimation error remains consistently low across short ranges and small azimuth angles, while it slightly increases at wider angles and larger ranges, where the SNR of the received pilots drops and the angular resolution decreases. It can be also seen that the isolated peaks with the smallest MLE values almost coincide with the blue markers signifying the true locations of the UEs, showcasing the effectiveness of both \mathbf{W}_{RX} designs. As demonstrated, on average, the projection-based solution outperforms the greedy-based one.

V. CONCLUSION

In this letter, we studied DMA-based reception for near-field localization, focusing on the THz frequency band. A novel expression for the CRB for the estimation of the UE range and angular parameters as well as the PEB were derived, and the former was deployed as the minimization objective for the design of the DMA analog RX BF weights. We capitalized on the partially-connected analog BF architecture of DMAs to reformulate its design objective into a Rayleigh quotient optimization problem with discrete constraints onto the analog BF weights, which was efficiently solved. Our simulation results verified the validity of our near-field localization analysis, showcasing the superiority

of our presented localization-optimized DMA design over conventional ones, when all implemented together with MLE.

REFERENCES

- [1] Z. Wang *et al.*, "A tutorial on extremely large-scale MIMO for 6G: Fundamentals, signal processing, and applications," *IEEE Commun. Surveys & Tuts.*, early access, 2024.
- [2] T. Gong *et al.*, "Holographic MIMO communications: Theoretical foundations, enabling technologies, and future directions," *IEEE Commun. Surveys & Tuts.*, vol. 26, no. 1, 2024.
- [3] H. Hua *et al.*, "Near-field integrated sensing and communication with extremely large-scale antenna array," *arXiv preprint arXiv:2407.17237*, 2024.
- [4] H. Chen *et al.*, "A tutorial on terahertz-band localization for 6G communication systems," *IEEE Commun. Surveys & Tuts.*, vol. 24, no. 3, 2022.
- [5] N. Shlezinger *et al.*, "Dynamic metasurface antennas for 6G extreme massive MIMO communications," *IEEE Wireless Commun.*, vol. 28, no. 2, pp. 106–113, 2021.
- [6] H. Zhang *et al.*, "Beam focusing for near-field multiuser MIMO communications," *IEEE Trans. Wireless Commun.*, vol. 21, no. 9, 2022.
- [7] K. Stylianopoulos *et al.*, "Autoregressive attention neural networks for non-line-of-sight user tracking with dynamic metasurface antennas," in *Proc. IEEE CAMSAP*, Los Sueños, Costa Rica, 2023.
- [8] P. Gavrilidis and G. C. Alexandropoulos, "Near-field beam tracking with extremely massive dynamic metasurface antennas," *arXiv preprint arXiv:2406.01488*, 2024.
- [9] Q. Yang *et al.*, "Near-field localization with dynamic metasurface antennas," in *Proc. IEEE ICASSP*, Rhodes, Greece, 2023.
- [10] I. Gavras *et al.*, "Full duplex holographic MIMO for near-field integrated sensing and communications," in *Proc. EUSIPCO*, Helsinki, Finland, 2023.
- [11] I. Gavras and G. C. Alexandropoulos, "Simultaneous near-field THz communications and sensing with full duplex metasurface transceivers," in *Proc. IEEE SPAWC*, Lucca, Italy, 2024.
- [12] S. Wang *et al.*, "A DOA estimation method based on low-complexity hybrid analog and digital architecture design," in *Proc. IEEE ICCT*, Bali, Indonesia, 2023.
- [13] T. Lin *et al.*, "Hybrid beamforming optimization for DOA estimation based on the CRB analysis," *IEEE Signal Process. Lett.*, vol. 28, 2021.
- [14] H. Qin *et al.*, "Cramér-Rao bound minimization for movable antenna-assisted multiuser integrated sensing and communications," *arXiv preprint arXiv:2407.11875*, 2024.
- [15] S. M. Kay, *Fundamentals of Statistical Signal Processing: Estimation Theory*. Prentice-Hall, Inc., 1993.
- [16] L.-H. Zhang, "On optimizing the sum of the Rayleigh quotient and the generalized Rayleigh quotient on the unit sphere," *Comput. Optimization Appl.*, vol. 54, no. 1, 2013.
- [17] I. J. Myung, "Tutorial on maximum likelihood estimation," *J. Math. Psychology*, vol. 47, no. 1, 2003.